 DOI: 10.3217/978-3-85125-528-7-09

Robust Blind Deconvolution Using Convolution Spectra of Images

Philipp Moser[1] and Martin Welk[1]

Biomedical Image Analysis Division
University for Health Sciences, Medical Informatics and Technology (UMIT),
Hall/Tyrol, Austria
philipp.moser@hotmail.com, martin.welk@umit.at

Abstract
We present a method for blind image deconvolution that acts by alternating optimisation of image and point-spread function. The approach modifies a variational model recently published by Liu et al. which combines a quadratic data term with a total variation regulariser for the image and a regulariser for the point-spread function that is constructed from convolution eigenvalues and eigenvectors of the blurred input image. We replace the image estimation component with a robust modification of Richardson-Lucy deconvolution, and introduce a robust data term into the point-spread function estimation. We present experiments on images with synthetic and real-world blur that indicate that the modified method has advantages in the reconstruction of fine image details.

1. Introduction

Blur is, second to noise, one of the major sources of degradations in digital images. Its removal has therefore been a subject of intense investigation since the beginnings of digital image processing. If for each location the intensity is smeared across a neighbourhood in the same way, this *spatially invariant* blur is mathematically modelled by a convolution with a kernel, called *point-spread function (PSF)*. Describing the observed blurred image f, the unobservable sharp image u and the PSF h as functions from suitable function spaces, and assuming additive noise n, one has

$$f = u * h + n \; . \tag{1}$$

Spatially variant blur can be modelled similarly using Fredholm integral operators. The mathematical problem of approximate inversion of these blur operations is termed deconvolution.

In this paper, we focus on the spatially invariant case. In *non-blind* deconvolution problems, both the blurred image f and the PSF h are available as input; in contrast, *blind* deconvolution aims at recovering the PSF h along with the sharp image u from the input image f. Both kinds of problems are severely ill-posed; in particular, deconvolution algorithms are highly sensitive to noise.

Non-blind deconvolution can nowadays be performed efficiently with favourable quality, with methods ranging from the time-proven Wiener filter [15] and Richardson-Lucy deconvolution [6, 10] up to the performant iterative algorithm by Krishnan and Fergus [4], to name a few representatives. Recently also neural network techniques have been used, see [12, 17].

For blind deconvolution, a straightforward approach proceeds in two steps: first, estimating the PSF,

and second, performing non-blind deconvolution with that PSF, see e.g. [3, 16]. Merging both steps, u and h can be estimated simultaneously by minimising a joint energy functional such as

$$E[u,h] := \int_\Omega (f - u * h)^2 \,\mathrm{d}\boldsymbol{x} + \alpha R_u[u] + \beta R_h[h] \;, \tag{2}$$

see e.g. [2, 11, 18], which combines the *data term* that integrates the squared model error $(f - u * h)^2$ over the image domain Ω with regularisation functionals R_u and R_h for the image and PSF, respectively, using regularisation weights α, β. Note that there is a formal symmetry between u and h in the data term, coming from the blur model (1); however, this symmetry usually does not extend to R_u and R_h – regularisers that work well for images do generally not perform favourably in PSF estimation, and vice versa. This is because the regularisers express model requirements for sharp images and for PSFs, respectively, and these model requirements differ substantially. For example, sharp edges are important for u which makes total variation regularisers a good candidate, whereas for h rather locality and sparse support may be meaningful requirements.

Motivated by the separation of regularisers in (2), one often separates u and h again in the minimisation, by using iterative methods that alternatingly update u and h. Each cycle then comprises an image estimation step, which is a non-blind deconvolution, and a PSF estimation step. Whereas the latter can formally be considered as non-blind deconvolution of the blurred image with respect to the sharpened image as convolution kernel, the dissimilarity of regularisers in fact often implies that substantially different algorithms have to be used for image and PSF estimation.

A refinement of (2) results from applying to the squared model error $(f - u * h)^2$ a function Φ with less-than-linear growth, yielding a sub-quadratic data term $\int_\Omega \Phi((f - u * h)^2) \,\mathrm{d}\boldsymbol{x}$. Data terms of this kind have been proven useful in various image processing tasks in order to reduce sensitivity to (particularly, heavy-tailed) noise and measurement errors as well as to minor deviations from the data model, and are therefore known as *robust data terms*, see e.g. [1, 19] in the deconvolution context. A similar modification of the objective function underlying the Richardson-Lucy deconvolution (the information divergence) has been introduced in [13], leading to a non-blind deconvolution method called robust and regularised Richardson-Lucy deconvolution (RRRL).

Our contribution. In this paper, important parts of which are based on the thesis [7], we review a recent blind deconvolution approach from [5] that is based on alternating minimisation of an energy in the sense of (2) with a PSF regulariser constructed from so-called convolution eigenvalues and eigenvectors. We then modify both the PSF and image estimation components of this approach by using robust data terms. To this end, we adopt in the image estimation component the RRRL method from [13]; regarding the PSF estimation component, we introduce a subquadratic data term. The so modified PSF estimation component has to the best of our knowledge not been studied before. We present experiments on a proof-of-concept level that support the conclusion that our modified method achieves higher reconstruction quality than its predecessor.

2. PSF Estimation Using Spectra of Convolution Operators

In this section, we review the approach from [5] which forms the basis for our further work in this paper. As the construction of the regulariser R_h from [5] relies on spectral decompositions formulated in matrix language, we switch our notations to use discrete images from here on.

Given a unsharp discrete grey-value image $\boldsymbol{f} = (f_{i,j})_{i,j}$, the sharp image $\boldsymbol{u}$ and the PSF $\boldsymbol{h}$ are sought as minimisers of the function (a discrete version of the functional (2))

$$E(\boldsymbol{u}, \boldsymbol{h}) := \sum_{i,j} (f_{i,j} - [\boldsymbol{u} * \boldsymbol{h}]_{i,j})^2 + \alpha R_u(\boldsymbol{u}) + \beta R_h(\boldsymbol{h}) \tag{3}$$

where in the discretised data term $[\boldsymbol{u} * \boldsymbol{h}]_{i,j}$ denotes the sampling value of the discrete convolution $\boldsymbol{u} * \boldsymbol{h}$ at location (i, j), and the regularisers R_u, R_h are still to be specified.

For the image, [5] use a total variation regulariser, which is common in literature, and known to produce favourable results in non-blind deconvolution. In discretised form it reads as $R_u(\boldsymbol{u}) = \sum_{i,j} \|[\boldsymbol{\nabla u}]_{i,j}\|$ where $[\boldsymbol{\nabla u}]_{i,j}$ denotes a discretisation of $\boldsymbol{\nabla} u$ at location (i, j). The central innovation of [5] lies in the PSF regulariser R_h which is built from *convolution eigenvalues and eigenvectors,* i.e. singular values and singular vectors of a linear operator associated with the image $\boldsymbol{f}$.

Note first that any discrete image $\boldsymbol{w}$, acting by convolution $\boldsymbol{w} * \boldsymbol{h}$ on the PSF, yields a linear operator on $\boldsymbol{h}$. In the discrete setting, we assume that the support of $\boldsymbol{h} = (h_{i,j})_{i,j}$ has size $m_x \times m_y$, which is embedded in a larger area $s_x \times s_y$ ([5] suggests $s_{x,y} \approx 1.5\, m_{x,y}$), and the discrete image $\boldsymbol{w}$ is of size $n_x \times n_y$. By discrete convolution with zero-padding, one has a linear operator $\boldsymbol{A}^{\boldsymbol{w}}_{s_x,s_y} : \boldsymbol{h} \mapsto \boldsymbol{w} * \boldsymbol{h}$ mapping $\mathbb{R}^{s_x \times s_y}$ to $\mathbb{R}^{(s_x+n_x-1)\times(s_y+n_y-1)}$ which has $s_x s_y$ (right) singular values $\sigma_k(\boldsymbol{w})$ with singular vectors $\boldsymbol{v}_k(\boldsymbol{w}) \in \mathbb{R}^{s_x \times s_y}$, which are called the convolution eigenvalues and eigenvectors of $\boldsymbol{w}$.

Theoretical analysis in [5] has brought out that, for meaningful convolution kernels $\boldsymbol{h}$, the convolution eigenvalues of $\boldsymbol{w} * \boldsymbol{h}$ are significantly smaller than those of $\boldsymbol{w}$; moreover, it is shown in [5] that particularly the convolution eigenvectors with smallest convolution eigenvalues of $\boldsymbol{w} * \boldsymbol{h}$ are almost convolution-orthogonal to $\boldsymbol{h}$, i.e. $\|\boldsymbol{v}_k(\boldsymbol{w} * \boldsymbol{h}) * \boldsymbol{h}\|$ is almost zero for those k for which $\sigma_k(\boldsymbol{w})$ is small enough. This motivates that for a given blurred image $\boldsymbol{f}$ the underlying PSF h can be sought as a minimiser of $\sum_{k=1}^{m_x m_y} \|\boldsymbol{v}_k(\boldsymbol{f}) * \boldsymbol{h}\|^2 / \sigma_k(\boldsymbol{f})^2$ where placing the squared convolution eigenvalues in the denominator ensures the higher influence of the convolution eigenvectors with smallest eigenvalues, and avoids introducing a threshold parameter to single out the "small" convolution eigenvalues.

An additional degree of freedom in the procedure is that the image $\boldsymbol{f}$ can be preprocessed by some linear filter L. Since convolution itself is a linear filter, and therefore commutes with any linear filter L, the above reasoning about singular values remains valid in this case; at the same time, a suitable choice of L allows to reweight the influence of different parts of $\boldsymbol{f}$ on the PSF estimation. Based on the well-known fact from literature, see e.g. [16], that edge regions are particularly well-suited to estimate blur, [5] suggest the use of a Laplacean-of-Gaussian (LoG) filter, thus leading to the final formulation of the objective function

$$R_h(\boldsymbol{h}) := \sum_{k=1}^{s_x s_y} \frac{\|\boldsymbol{v}_k(L(\boldsymbol{f})) * \boldsymbol{h}\|^2}{\sigma_k(L(\boldsymbol{f}))^2} \tag{4}$$

where L is a LoG operator. Whereas the extended support size $s_x \times s_y$ for $\boldsymbol{h}$ is used in R_h, its minimisation is constrained to PSF $\boldsymbol{h}$ of the actual support size $m_x \times m_y$.

Using R_h alone as objective function would already allow to estimate the PSF fairly accurate. However, as discussed in [5] such a proceeding tends toward some over-sharpening of the image with visible artifacts. In order to achieve a good joint reconstruction of the sharp image and PSF that also takes into account regularity constraints on the image expressed by R_u, and improves the treatment of images with moderate noise, [5] insert R_h instead as PSF regulariser into (3).

This joint energy functional is then minimised by an alternating minimisation. In the PSF estimation step, $R_h(\boldsymbol{h})$ is represented as a quadratic form, $R_h(\boldsymbol{h}) = \sum_{i,j,i',j'} H_{i,j;i',j'} h_{i,j} h_{i',j'}$, with the coefficient matrix (Hessian) $\boldsymbol{H} = (H_{i,j;i',j'})_{i,j,i',j'}$ given by

$$\boldsymbol{H} = \sum_{k=1}^{s_x s_y} \frac{\boldsymbol{A}_{m_x,m_y}^{\boldsymbol{v}_k(L(\boldsymbol{f}))\mathrm{T}} \boldsymbol{A}_{m_x,m_y}^{\boldsymbol{v}_k(L(\boldsymbol{f}))}}{\sigma_k(L(\boldsymbol{f}))^2} \ , \tag{5}$$

and this is combined with the data term from (3) to establish a quadratic minimisation problem for $\boldsymbol{h}$.

In our re-implementation of the PSF estimation from [5], this quadratic minimisation problem is solved via the corresponding linear equation system and an LU decomposition [9, pp. 52p.], followed by a projection step that eliminates negative entries in $\boldsymbol{h}$ and normalises $\boldsymbol{h}$ to unit total weight. As a refinement of the projection step, it turned out useful to cut off even small positive entries in $\boldsymbol{h}$ by a threshold, thus additionally enforces sparsity of the PSF. Experiments indicate that the threshold is best adapted as a multiple of some quantile, e.g. 0.1 times the $95\,\%$-quantile of the entries of $\boldsymbol{h}$.

The image estimation step that alternates with PSF estimation comes down to a TV-regularised non-blind deconvolution problem for which several approaches exist. In [5] the method from [4] is used.

3. Robust Image and PSF Estimation

As demonstrated in e.g. [1, 8, 14, 13], robust data terms allow to achieve favourable deconvolution results even with imprecise estimates of the PSF or slight deviations from the spatial invariant blur model. While the latter is generally relevant in deconvolution of real-world images, robustness to imprecise PSF estimates is particularly useful in blind deconvolution. This makes it attractive to incorporate robust data terms into the framework of [5], which is our goal in this section.

Due to the alternating minimisation structure of the method, we consider the two steps separately. We start with the image estimation, which is tantamount to non-blind deconvolution. Thus, we simply have to replace the TV deconvolution model with a suitable robust approach. In this work, we choose RRRL [13] for this purpose, which is a fixed point iteration associated to the energy function

$$E(\boldsymbol{u}) = \sum_{i,j} \Phi\left([\boldsymbol{u} * \boldsymbol{h}]_{i,j} - f_{i,j} - f_{i,j} \ln \frac{[\boldsymbol{u} * \boldsymbol{h}]_{i,j}}{f_{i,j}} \right) \mathrm{d}\boldsymbol{x} + \alpha R_u(\boldsymbol{u}) \ . \tag{6}$$

We prefer this method for efficiency reasons; note that the non-blind deconvolution step is needed in each iteration of the alternating minimisation. RRRL is known to evolve fast toward a good solution during the first few iterations, see also [14], whereas methods based on approaches as in [1] tend to require more iterations. Following [13], the data term penaliser in the RRRL method is chosen as $\Phi(z) = 2\sqrt{z}$, whereas the image regulariser R_u is chosen as total variation as in Section 2.

For the PSF estimation, we insert a penaliser function Φ as mentioned above into the discretised data term from (3), which is then combined with the unaltered regulariser R_h from (4) to yield a (partial) discrete energy function for the estimation of $\boldsymbol{h}$:

$$E(\boldsymbol{h}) = \sum_{i,j} \Phi\big((f_{i,j} - [\boldsymbol{u} * \boldsymbol{h}]_{i,j})^2 \big) \, \mathrm{d}\boldsymbol{x} + \alpha R_h(\boldsymbol{h}) \ . \tag{7}$$

Unlike its counterpart in Section 2., this energy function is no longer quadratic. Equating the gradient (i.e. the derivatives w.r.t. $h_{i,j}$) to zero now yields a system of nonlinear equations for the PSF entries.

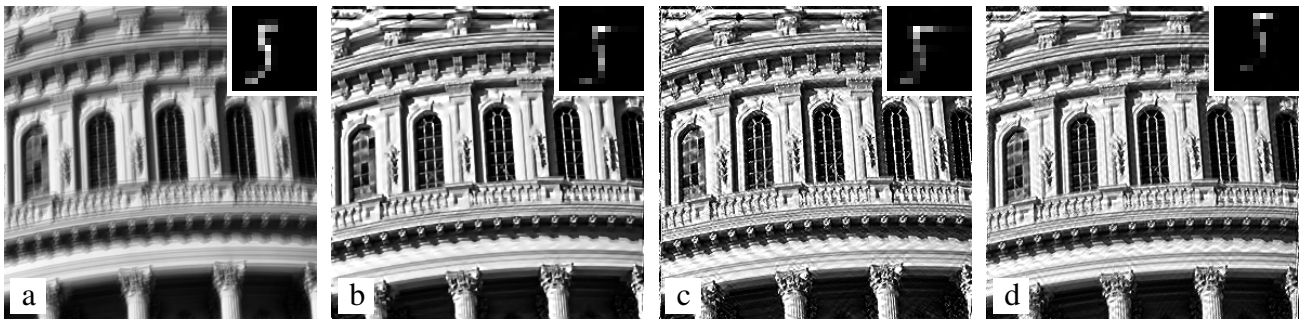

Figure 1. Blind deconvolution of a synthetically blurred image. (a) Input image, 289×289 pixels, blurred with the PSF, 13×13 pixels, shown as insert. From [5], adapted. – (b) Reconstructed image and PSF (inserted) by the method from [5], $m_x = m_y = 13$, $\beta = 5050$, $K = 200$. – (c) Same as (b) but with RRRL used in the image estimation step, $\alpha = 0.0018$, $K_u = 30$. – (d) Same as (b) but with RRRL for image estimation, and the nonlinear PSF estimation method from Section 3., $\alpha = 0.0018$, $\beta = 5050$, $K_u = 30$, $K_h = 20$. – For τ, the quantile criterion (see Section 2.) was used in (c, d) and yielded values in the range $0.11 \ldots 0.12$. (b)–(d) from [7], adapted.

By a standard procedure of lagged weights (analogous to the lagged diffusivity method or Kačanov method) we transform the nonlinear equation system into a sequence of linear ones. Note that the nonlinearities result from the terms $\partial_{h_{p,q}} \Phi\big((f_{i,j} - [\boldsymbol{u} * \boldsymbol{h}]_{i,j})^2\big) = -2\Phi'\big((f_{i,j} - [\boldsymbol{u} * \boldsymbol{h}]_{i,j})^2\big)(f_{i,j} - [\boldsymbol{u} * \boldsymbol{h}]_{i,j}) u_{i-p,j-q}$. Starting with some initial approximation $\boldsymbol{h}^0$ for $\boldsymbol{h}$, we proceed therefore for $l = 0, 1, 2, \ldots$ as follows: Compute the weights $\varphi_{i,j}^l := \Phi'\big((f_{i,j} - [\boldsymbol{u} * \boldsymbol{h}^l]_{i,j})^2\big)$ and replace $\Phi'(\,\cdot\,)$ in the equation system with the fixed $\varphi_{i,j}$. This gives a linear equation system for $\boldsymbol{h}$. Applying LU decomposition as in Section 2. one computes the solution $\boldsymbol{h}^{l+1}$ of this system, which is the starting point for the next iteration. A more spelled-out derivation of the sequence of linear equation systems is found in [7]. Experimental evidence in [7], see also Section 4., confirms the quick convergence of the sequence $(\boldsymbol{h}^l)$; in practical cases, often $10 \ldots 20$ iterations are sufficient.

To end the description of our robust blind deconvolution method, we summarise its parameters which will also be referred to in Section 4. The original method from [5] and the version with RRRL and linear PSF estimation use obvious subsets of these parameters. We start by the model parameters. First, there are the PSF sizes m_x, m_y that need to be chosen somewhat larger than the actual PSF. For the sample sizes s_x, s_y we adopt the heuristic choice $s_{x,y} \approx 1.5\, m_{x,y}$ from [5]. Regarding the image regularisation weight α in (6), a continuation strategy that starts with a larger α in the first iterations of the alternating minimisation and reduces α during the alternating minimisation process helps to speed up convergence; the final values of α lie in the range $\alpha \approx 0.001 \ldots 0.002$ proposed in [13]. The PSF regularisation weight β is set manually; if it is too small, the blur will be underestimated (with a point kernel as extreme); too large β leads to oversharpening, compare [5]. Finally, there is the threshold τ for the PSF entries. The essential numerical parameters are three iteration counts: K for the alternating minimisation, K_u for RRRL, and K_h for the iterated linearisation of the nonlinear equation system in the PSF estimation.

4. Experiments

As a proof of concept, we present two experiments here; further experiments can be found in [7]. Our first experiment is based on a synthetically blurred image, Fig. 1(a), that was already used in [5] to exemplify the method reviewed in Section 2. The result of this method is shown in Figure 1(b). Frame (c) has been obtained by replacing the image estimation component with RRRL, whereas in frame (d) also the robust PSF estimation from Section 3. has been employed. Comparing (b) and (c), it is

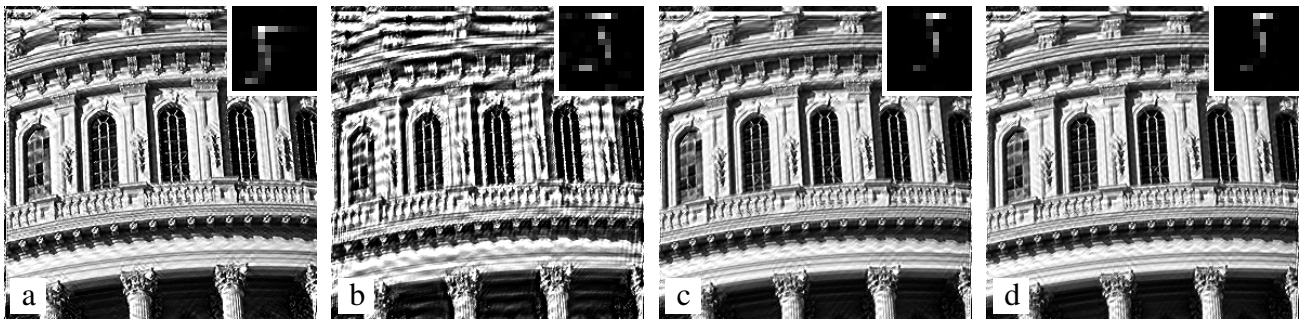

Figure 2. Blind deconvolution of the synthetically blurred image from Fig. 1(a) using RRRL for image estimation, and the nonlinear PSF estimation method from Section 3. with different numbers of linearisation iterations. (a) 1 iteration. – (b) 2 iterations. – (c) 5 iterations. – (d) 8 iterations. – From [7], adapted.

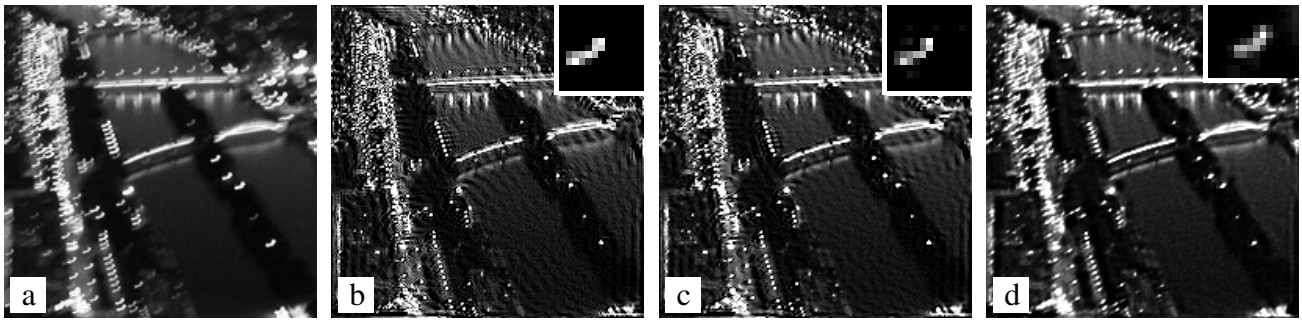

Figure 3. Blind deconvolution of an image blurred during acquisition. (a) Clipping from a photograph (Paris from Eiffel tower at dusk) blurred by camera shake, 200×200 pixels. – (b) Reconstructed image and PSF, 13×13 pixels (inserted), using RRRL for image estimation and PSF estimation according to [5], $m_x = m_y = 13$, $\alpha = 0.002$, $\beta = 260$, $\tau = 0.1$, $K = 300$, $K_u = 20$. – (c) Same as (b) but with nonlinear PSF estimation Section 3., $m_x = m_y = 13$, $\alpha = 0.0105$, $\beta = 255$, $\tau = 0.1$, $K = 300$, $K_u = 20$, $K_h = 8$. – (d) Non-blind RRRL deconvolution result with the manually tuned PSF (shown as insert) from [13], $\alpha = 0.002$, $K_u = 30$. The PSF, 14×11 pixels, has been generated from an impulse response.

evident that introducing robust image estimation brings about a slight gain in reconstruction of small detail, but also an amplification of artifacts is observed which may be attributable to the mismatch between the data terms underlying the PSF estimation (non-robust) and non-blind deconvolution (robust). Using robust estimation methods for both (d) leads to a result with visible gain in sharpness and fewer artifacts. In particular, fine details of the columns between the windows are reconstructed sharper in (d) than in (b). Regarding the visible translation by approx. 2 pixels between (d) and the two other results, it should be noted that shifting the PSF and image in opposing directions is an inherent degree of freedom of the convolution model (1). Note that this also poses a difficulty for quantitative evaluation of blind deconvolution methods: quantitative error measurements cannot be done without a registration step whose influence on the error values needs additional analysis. Since this is not feasible within the present paper, we restrict ourselves to a visual assessment at this point.

As discussed in Section 3. the non-linear system of equations arising in the PSF estimation is solved iteratively by linearisation. In Fig. 2 we demonstrate the evolution of estimated PSF and image with increasing number of linearisation iterations. With a single iteration, frame (a), the result is almost identically to the linear PSF estimation from Fig. 1(c). Additional iterations first lead to some artifacts, frame (b), which are apparently caused by the fact that the non-linear method places the PSF in this example at a translated position. With more iterations, the reconstruction quickly stabilises at the refined result, frame (d), which is numerically converged and corresponds to Fig. 1(d).

In our last experiment, Fig. 3, we consider an image blurred by camera shake. The test image, Fig. 3 (a), is clipped from a test image used in [13] to demonstrate the non-blind RRRL method. In [13] it was used in conjunction with a PSF manually generated from an impulse response (the image of a street light); we reproduce this experiment from [13] in frame (d) for reference. In frames (b) and (c) we show blind deconvolution results: frame (b) again combines RRRL for image estimation with the linear PSF estimation from [5], whereas (c) employs also the robust PSF estimation from Section 3. It is evident that in (c) the estimated PSF has become sharper, and artifacts in the deblurred image have been reduced, although the reconstruction quality is still not quite on par with the non-blind result (d).

5. Summary and Outlook

In this paper we have shown how a recent blind image deconvolution approach by alternating minimisation of a joint energy functional [5] can be improved by introducing robust methods for PSF and image estimation. For image estimation we used RRRL [13], whereas for PSF estimation a modification of the method from [5] has been used that is, to best of our knowledge, new. The viability of the approach has been demonstrated on synthetic and real-world blurred images.

A weakness of this combination of methods is that the robust data terms used in the image and PSF estimation differ, compare (6), (7), and cannot be cast into a joint energy functional. This is a pragmatic decision justified by the efficiency of RRRL and the fact that, as demonstrated in [13], its results in non-blind deconvolution are largely comparable with those of a method in the sense of [1] whose data term is compatible with (7). Notwithstanding, it will be a goal of future work to reformulate the robust model such that PSF and image estimation can be expressed in a unified functional. It is expected that an exact match of data terms will also further reduce artifacts in the blind deconvolution results.

The present paper is restricted to grey-value images; an extension to multi-channel (colour) images will be detailed in a forthcoming publication. Future work might also address strategies for the choice of parameters as well as efficiency improvements of the algorithm. In order to further study the practical applicability of the method, experimental validation using larger sets of images will be important, including quantitative comparisons. Moreover, we have focussed in this work on the ability of robust data terms to cope with imprecise PSF estimation and model violations, but largely ignored their potential in treating strong noise. Experiments on noisy blurred images will deepen insight into this aspect.

References

[1] L. Bar, N. Sochen, and N. Kiryati. Image deblurring in the presence of salt-and-pepper noise. In R. Kimmel, N. Sochen, and J. Weickert, editors, *Scale Space and PDE Methods in Computer Vision*, volume 3459 of *Lecture Notes in Computer Science*, pages 107–118. Springer, Berlin, 2005.

[2] T. F. Chan and C. K. Wong. Total variation blind deconvolution. *IEEE Transactions on Image Processing*, 7:370–375, 1998.

[3] R. Fergus, B. Singh, A. Hertzmann, S. T. Roweis, and W. T. Freeman. Removing camera shake from a single photograph. In *Proc. SIGGRAPH 2006*, pages 787–794, New York, NY, July 2006.

[4] D. Krishnan and R. Fergus. Fast image deconvolution using hyper-Laplacian priors. In *Advances in Neural Information Processing Systems*, pages 1033–1041, 2009.

[5] G. Liu, S. Chang, and Y. Ma. Blind image deblurring using spectral properties of convolution operators. *IEEE Transactions on Image Processing*, 23(12):5047–5056, 2014.

[6] L. B. Lucy. An iterative technique for the rectification of observed distributions. *The Astronomical Journal*, 79(6):745–754, June 1974.

[7] P. Moser. Blind image deblurring using the deconvolution operator's spectral properties and non-linear kernel estimation. Master's thesis, UMIT, Hall/Tyrol, Austria, 2015.

[8] N. Persch, A. Elhayek, M. Welk, A. Bruhn, S. Grewenig, K. Böse, A. Kraegeloh, and J. Weickert. Enhancing 3-D cell structures in confocal and STED microscopy: a joint model for interpolation, deblurring and anisotropic smoothing. *Measurement Science and Technology*, 24(12):125703, 2013.

[9] W. H. Press, S. A. Teukolsky, W. T. Vetterling, and B. T. Flannery. *Numerical Recipes. The Art of Scientific Computing. Third Edition*. Cambridge University Press, Cambridge, 2007.

[10] W. H. Richardson. Bayesian-based iterative method of image restoration. *Journal of the Optical Society of America*, 62(1):55–59, 1972.

[11] K. Schelten, S. Nowozin, J. Jancsary, C. Rother, and S. Roth. Interleaved regression tree field cascades for blind image deconvolution. In *IEEE Winter Conference on Applications of Computer Vision*, pages 494–501, 2015.

[12] C. J. Schuler, H. C. Burger, S. Harmeling, and B. Schölkopf. A machine learning approach for non-blind image deconvolution. In *IEEE Conference on Computer Vision and Pattern Recognition (CVPR)*, pages 1067–1074, 2013.

[13] M. Welk. A robust variational model for positive image deconvolution. *Signal, Image and Video Processing*, 10(2):369–378, 2016.

[14] M. Welk, P. Raudaschl, T. Schwarzbauer, M. Erler, and M. Läuter. Fast and robust linear motion deblurring. *Signal, Image and Video Processing*, 9(5):1221–1234, 2015.

[15] N. Wiener. *Extrapolation, Interpolation and Smoothing of Stationary Time Series with Engineering Applications*. MIT Press, Cambridge, MA, 1949.

[16] L. Xu and J. Jia. Two-phase kernel estimation for robust motion deblurring. In K. Daniilidis, P. Maragos, and N. Paragios, editors, *Computer Vision – ECCV 2010, Part I*, volume 6311 of *Lecture Notes in Computer Science*, pages 157–170. Springer, Berlin, 2010.

[17] L. Xu, J.SJ. Ren, C. Liu, and J. Jia. Deep convolutional neural network for image deconvolution. In *Advances in Neural Information Processing Systems*, pages 1790–1798, 2014.

[18] Y.-L. You and M. Kaveh. Anisotropic blind image restoration. In *Proc. 1996 IEEE International Conference on Image Processing*, volume 2, pages 461–464, Lausanne, Switzerland, September 1996.

[19] M. E. Zervakis, A. K. Katsaggelos, and T. M. Kwon. A class of robust entropic functionals for image restoration. *IEEE Transactions on Image Processing*, 4(6):752–773, June 1995.